Applied Catalysis B: Environmental 127 (2012) 291–299

Contents lists available at SciVerse ScienceDirect

Applied Catalysis B: Environmental

journal homepage: www.elsevier.com/locate/apcatb

Carbon nanofibres as substrates for the preparation of TiO_2 nanostructured photocatalysts

M. Ouzzine, M.A. Lillo-Ródenas*, A. Linares-Solano

Grupo de Materiales Carbonosos y Medioambiente, Dpto. Química Inorgánica, Facultad de Ciencias, Universidad de Alicante, Ap. 99, E-03080 Alicante, Spain

ARTICLE INFO

Article history:
Received 16 April 2012
Received in revised form 14 August 2012
Accepted 28 August 2012
Available online 5 September 2012

Keywords:
Titanium dioxide
Carbon nanofibres
Photocatalytic activity
Propene

ABSTRACT

Carbon nanofibres from different origins have been used as substrates for the preparation of TiO_2/CNF hybrid materials and TiO_2 nanofibres. The influence of the CNFs on the final properties of the prepared materials is analysed. The results show that the crystallinity of the CNFs used is the parameter that most influences the quality of the TiO_2 deposition. CNFs with low-to-moderate crystallinities are suitable for preparing TiO_2/CNF materials with a uniform TiO_2 coating and with interesting properties: high surface areas, close to 400 m^2/g, and anatase phase. Additionally, TiO_2 nanofibres maintaining such anatase phase and an important surface area can be prepared from these uniform TiO_2/CNF hybrids by burning the CNFs. These TiO_2/CNF hybrid materials and TiO_2 nanofibres, having larger surface areas than similar materials prepared in a previous work using carbon nanotubes, are analysed as photocatalysts for the oxidation of propene at low concentration (100 ppmv) under UV light irradiation. The results show interesting photocatalytic activities (better for the hybrid materials than for the TiO_2 nanofibres), that can be further enhanced increasing the surface area and/or reaching a suitable anatase/rutile proportion.

1. Introduction

TiO_2 has been one of the most widely investigated and used materials over the past decades because it is nontoxic, easy to be made, inexpensive and chemically stable [1–3].

In recent years, TiO_2-based materials have attracted significant research attention due to their broad applications in the fields of water and air purification [4,5], hydrogen evolution [6], CO_2 photoreduction [7], dye sensitised solar cells [8] and sensor devices [9]. However, the large band gap in TiO_2 and high recombination rate of the photogenerated electron/hole pairs hinder further applications in industry [10].

In the field of photocatalysis, many efforts have been attempted to improve activity of TiO_2. One of the alternatives studied is based on immobilising TiO_2 on different substrate materials [6–9,11–21], which mostly include carbon materials [6–9,11,13–17], but also glass [12] or zeolites [20,21]. Among the different carbon materials studied, carbon nanotubes (CNTs) have been the preferred ones [6–9,14–17] due to their extraordinary mechanical and electronic properties and because they can be semiconducting [22].

In addition, CNTs have good adsorption capacity and uniform pore structure [23], which is an advantage for photocatalytic applications. These TiO_2/CNT hybrid materials have exhibited better photocatalytic performance than pure TiO_2 [6,14–16] due to two positive effect of the carbon nanotubes; (i) they provide a surface area that prevents charge recombination by trapping photo-excited electrons generated from TiO_2 [14] and (ii) they have conducting properties that help the transfer of electrons from TiO_2 to CNTs, enhancing the oxidative reactivity [14].

Thus, in a recent study [16] we have obtained promising photocatalytic activity for a TiO_2/CNT hybrid material prepared by sol–gel method, although its resulting specific surface area was low. To improve these results another nanostructured carbon material, with higher surface area, e.g. carbon nanofibres, has recently been investigated for the preparation of TiO_2-based materials, with positive results [17–19]. However, the influence of the properties of the CNFs on the resulting TiO_2/CNF hybrid materials was not investigated.

The present paper deals with the following objectives: (i) the preparation of TiO_2/CNF hybrid materials, paying attention to the properties of the CNFs used as substrates, mainly their structural order, porosity and surface chemistry, (ii) the preparation of high surface area TiO_2 nanofibres from the synthesised TiO_2/CNF hybrid materials, and (iii) an analysis of the photocatalytic application of the samples prepared in this study, evaluated by the photocatalytic

* Corresponding author. Tel.: +34 965909350; fax: +34 965903454.
E-mail address: mlillo@ua.es (M.A. Lillo-Ródenas).

0926-3373/$ – see front matter © 2012 Elsevier B.V. All rights reserved.
http://dx.doi.org/10.1016/j.apcatb.2012.08.029

oxidation (PCO) of propene under UV irradiation carried out in the gas phase at low concentration (100 ppmv).

2. Materials and methods

2.1. Carbon nanofibres

Three commercial carbon nanofibres (CNFs) have been selected to study their influence as substrates on the preparation of the TiO_2/CNF hybrids: Gun-ei (Gun-ei Chemical Ind. Co. Ltd., Japan), Pyrograph III (Pyrograph Products Inc., Cedarville, OH, USA) and GANF (Grupo Antolín Ingenieria, Spain). These CNF materials will be referred to as Gun-ei, Pyrograph and GANF.

Additionally, GANF and Gun-ei nanofibres were oxidised with nitric acid. For such surface oxidation, pristine GANF and Gun-ei CNFs were in contact with a nitric acid solution (HNO_3, 4 M) under stirring for 2 h at room temperature. The ratio CNF/nitric acid solution was 1 g of CNF for 20 ml of the acid solution. These acid-treated CNFs, named Gun-ei-ox and GANF-ox, were washed with deionised water until pH value being neutral and dried in an oven at 100 °C for 24 h.

2.2. Synthesis of TiO_2/CNF hybrids

Five TiO_2/CNF hybrids were prepared by sol–gel route using tetrabutyl titanate ($Ti(OBu)_4$) as follows [24]: firstly, the CNFs (Gun-ei, Pyrograph, GANF, Gun-ei-ox and GANF-ox) were dispersed into ethanol by ultrasonication for 15 min, previously to the addition of $Ti(OBu)_4$. Then, after strong stirring at room temperature for 1 h, a mixture of HCl and ethanol was added drop wise into the suspension; the mixture was continuously stirred for 1 h. Finally, the TiO_2/CNF materials were prepared by filtering and drying at 100 °C for 24 h. This procedure was repeated for eight times. A final heat treatment at 300 °C in a muffle was performed to induce crystallinity in the TiO_2 samples. The TiO_2/CNF hybrid materials are labelled using the CNF substrate name (as an example, TiO_2/Gun-ei).

2.3. Synthesis of TiO_2 nanofibres

The TiO_2 nanofibres were synthesised from the previously prepared TiO_2/CNF hybrids by burning out the CNFs. Thus, the TiO_2/CNF hybrids were placed in a muffle and heated at 10 °C/min rate up to 450–550 °C for 3 h to remove the carbon nanofibres. The TiO_2 nanofibres were labelled as NF-TiO_2 followed by the name of the nanofibre that was previously used as substrate. As an example, NF-TiO_2-Gun-ei corresponds to TiO_2 nanofibres that have been prepared from TiO_2/Gun-ei burning Gun-ei CNFs in air.

2.4. Characterisation of the samples

The carbon nanofibres, TiO_2/CNF hybrid materials and TiO_2 nanofibres were characterised as follows: (1) their porous texture was analysed by nitrogen and carbon dioxide adsorption at −196 °C and 0 °C, respectively, using an Autosorb-6B apparatus from Quantachrome. BET surface area (S_{BET}) was calculated applying the BET equation to N_2 adsorption data [25]. Total micropore volume (porosity below 2 nm width, referred to as DR N_2) was determined by application of the Dubinin–Radushkevich equation to the N_2 adsorption data [25]. The narrow micropore volume (porosity below 0.7 nm width, referred to as DR CO_2) was determined by the application of the Dubinin–Radushkevich equation to the CO_2 adsorption data [26,27]; (2) the surface chemistry of the CNFs was studied by temperature programmed desorption (TPD) experiments carried out over the CNFs using a DSC-TGA equipment (Simultaneous DSC-TGA SDT 2960, TA Instruments) coupled to a mass spectrometer (Thermostar, Balzers). In these experiments, 10 mg of sample were heated to 900 °C (heating rate 20 °C/min) under a helium flow rate of 100 ml/min; (3) the reactivity of the CNFs in air was analysed by thermogravimetric analysis (simultaneous DSC-TGA SDT 2960, TA Instruments), heating at 10 °C/min from room temperature to 900 °C; (4) their structures were characterised by powder X-ray diffraction (XRD). The XRD patterns were recorded using a SEIFERT 2002 equipment as well as a Bruker D8 Advance (40 kV/40 mA) with Cu Kα (α = 1.54 Å) radiation. The scanning velocity was 2°/min and the 2θ range scanned ranged from 6° to 80°. The crystalline size of the different titanium dioxide crystalline phases was determined by the Scherrer formula, using a K factor of 0.93:

$$B = \frac{K\lambda}{\beta \cos\theta} \quad (1)$$

where B is the crystalline size (nm); λ the wavelength of the radiation used, which is 1.54056 Å for Cu; β the full width at half maximum intensity (FWHM); and θ is the angle for the XRD maximum peak. (5) The sample morphology was studied by scanning electronic microscopy (SEM) using JEOL JSM-840 and transmission electron microscopy (TEM) using INCA Energy TEM100 equipment from OXFORD Instruments. Thus, SEM and TEM of the hybrid samples were used, among others, to determine if a homogeneous TiO_2 covering has been obtained. The measurement and calculation of mean diameters of the hybrid materials and TiO_2 nanofibres was performed by the software analiSIS. (6) The TiO_2 content in the hybrid materials was determined by burning some portion of these samples in a muffle up to 900 °C and comparing the weight of the samples before and after such burning step.

2.5. Experimental conditions for propene oxidation at low concentration

The photocatalytic activities of TiO_2/CNFs and TiO_2 nanofibres were evaluated by photocatalytic oxidation (PCO) of propene, which is one of the major sources of both outdoor (it is involved in vehicle emissions and in many industrial applications, such as in petrochemical plants and foundry operations) as well as of indoor air pollution. So far, few studies have been reported on the photocatalytic oxidation of propene in gas phase using TiO_2 [16,28–30,32], despite the fact that it is one of the main components of tobacco smoke [28,31].

The experimental system used was designed in our laboratory. It consists of a quartz reactor provided by AFORA where the photocatalyst bed is placed on quartz wool. A Philips UV lamp is placed parallel to the quartz reactor, at around 1 cm. The UV lamp radiation peak appears at 257.7 nm (UV-C). The commercial reference of the lamp is TUV 8W FAM. The couple quartz reactor-lamp is surrounded by a cylinder covered by tinfoil. A scheme of this system is detailed elsewhere [32].

The weight of photocatalyst used in these experiments was 0.11 g for the TiO_2 nanofibres and, for comparison purposes, different TiO_2/CNF sample weights were used to maintain a constant 0.11 g mass of TiO_2.

These photocatalysts were used for the oxidation of propene at 100 ppmv in air at room temperature, 25 °C. Two flow rates of the propene stream, 30 and 60 ml/min (STP), were tested. These flow rates were controlled by automated mass flow-controllers (Brook Instruments). After suitable calibrations, a mass spectrometer (Balzers, Thermostar GSD 301 01) coupled to the outlet of the reactor bed follows the evolution of the concentration of propene in the outlet gas with time. The experiments were repeated at least

Table 1
Characterisation of the carbon nanofibres.

Sample	S_{BET} (m^2/g)	DR N_2 (cm^3/g)	DR CO_2 (cm^3/g)	CO (μmol/g)	CO_2 (μmol/g)
Pyrograph	44	0.02	0.00	344	340
GANF	178	0.06	0.03	548	409
Gun-ei	493	0.21	0.25	1678	900

two times for checking reproducibility. Propene conversion was calculated using the following expression:

$$\text{Propene conversion}\,(\%) = \frac{C_{\text{initial C3H6}} - C_{\text{stationary C3H6}}}{C_{\text{initial C3H6}}} \times 100 \qquad (2)$$

where $C_{\text{initial C3H6}}$ is the initial propene concentration, 100 ppmv, and $C_{\text{stationary C3H6}}$ is the stationary propene concentration in the photocatalyst bed outlet gas when the UV source is switched on.

The amount of CO_2 after the oxidation was quantified by mass spectrometry, using a calibrated CO_2-cylinder with a concentration of 300 ppmv.

3. Results and discussion

3.1. Characterisation of the CNFs

As detailed in the experimental section, three carbon nanofibres were selected for preparation of the TiO_2/CNF samples. Table 1, which summarises the textural characteristics and the surface chemistry of the three pristine CNFs, shows that the samples strongly differ in terms of surface areas, microporosity and oxygen surface chemistry, being samples Gun-ei and Pyrograph the two extreme ones. Gun-ei presents the largest porosity, surface area and oxygen content, whereas Pyrograph is the one with lowest porosity, surface area and oxygen content.

Fig. 1 shows adsorption/desorption isotherms of N_2 at −196 °C for the three CNFs. Gun-ei and Gun-ei-ox CNFs show type I isotherms, according to IUPAC classification [33] and their shapes indicate that these materials contain an important amount of narrow micropores. Fig. 1 also shows that Pyrograph and GANF have type II isotherms with H3 hysteresis cycles (according to IUPAC classification) [33]. These isotherms indicate that these materials are non-porous or macroporous. The presence of H3 hysteresis is due to the presence of some mesoporosity.

Fig. 2 shows the XRD patterns of the three pristine CNFs. The X-ray diffractogram of GANF and Pyrograph present two main peaks centred at 2θ values of 26.5° and 44°, which correspond to (0 0 2) and (1 0 1) set of planes of graphite, respectively, having sample GANF sharper peaks than Pyrograph. Additionally, the (0 0 2) peak of Pyrograph is asymmetric. Contrarily, the XRD patterns of Gun-ei do not show peaks (or bands), indicative of its amorphous structural character. Thus, from the XRD patterns it can be concluded that the structural order increases from Gun-ei to Pyrograph and to GANF, as it has been previously reported [34].

3.2. Morphology of the prepared TiO_2/CNF samples

TiO_2/CNF hybrid materials have been prepared by the sol–gel method already described, using the three pristine CNFs as substrates. The morphology of the prepared hybrids was investigated with transmission electron microscopy (TEM) (Fig. 3a–c).

Fig. 3 shows that TiO_2 is more homogeneously and densely spread on the surfaces of Gun-ei and Pyrograph than in the most crystalline nanofibres, GANF. These results seem to indicate that neither porosity nor surface chemistry are the parameters most influencing the homogeneity of the TiO_2 layer deposited on the CNFs, since GANF nanofibres present intermediate porosity and surface chemistry values (between those of Pyrograph and Gun-ei). Contrarily, the structural order seems to be the key parameter for achieving a uniform deposition of TiO_2. A high structural order, as in the case of GANF, makes difficult a homogeneous covering of the nanofibres by TiO_2.

For TiO_2/Gun-ei and TiO_2/Pyrograph the TiO_2 weight percentages are 27 and 43 wt.%, respectively, determined by TG analysis up to 900 °C in air. In the case of TiO_2/GANF, the weight percentage of TiO_2 is 86 wt.%, which indicates that a much larger amount of TiO_2 is deposited in this most ordered nanofibre, although not forming a uniform deposited layer of TiO_2. Additionally, and in agreement with previous results, it can be concluded that crystallinity of the CNF support induces the largest amount of TiO_2 deposited, but does not favour the formation of a uniform layer of TiO_2 over the nanofibres.

3.3. TiO_2/CNF-ox samples

Because a uniform layer of TiO_2 covering on the GANF nanofibres could not be obtained, pre-oxidation of these carbon nanofibres (samples GANF-ox) has been carried out trying to improve the covering. For comparative purpose, the sample Gun-ei has also been oxidised as well (Gun-ei-ox). These two oxidised samples were

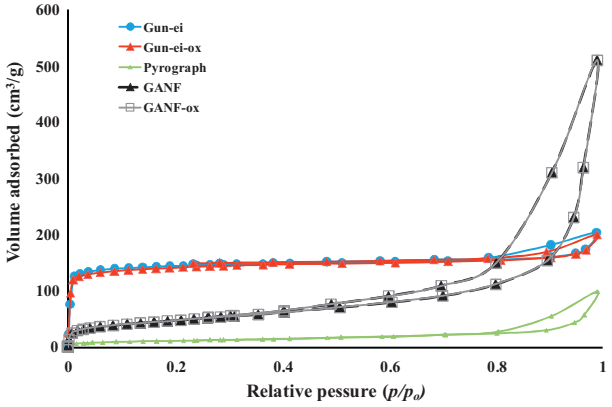

Fig. 1. Adsorption–desorption isotherms of N_2 at −196 °C on the original CNF substrates, Gun-ei, Gun-ei-ox, Pyrograph, GANF and GANF-ox.

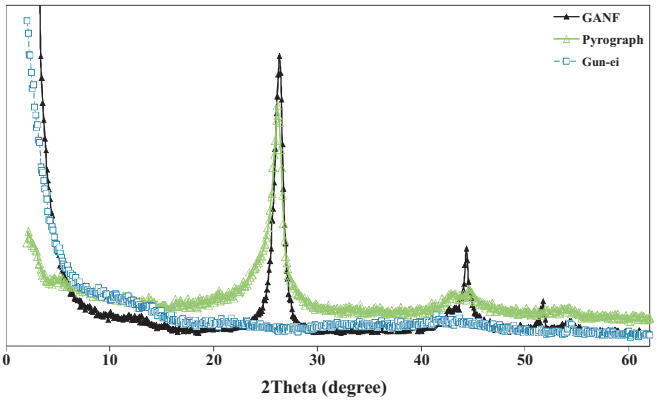

Fig. 2. X-ray diffractograms of pristine CNFs: GANF, Pyrograph and Gun-ei.

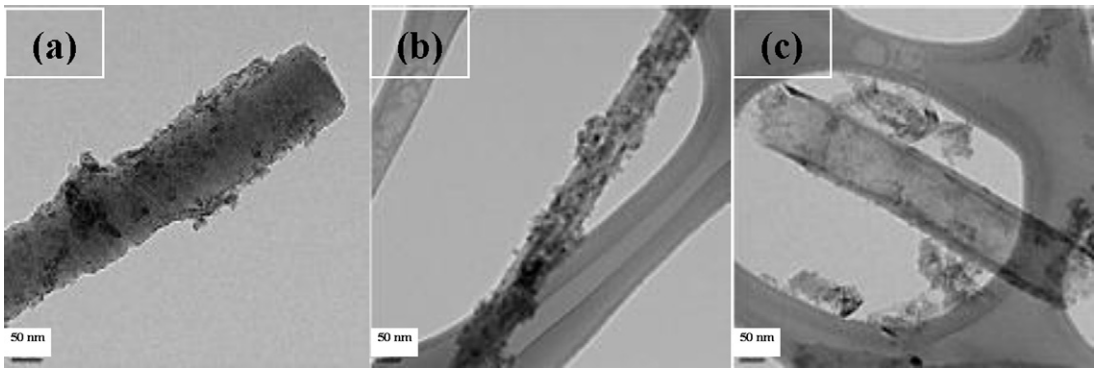

Fig. 3. TEM images of (a) TiO_2/Gun-ei; (b) TiO_2/Pyrograph; and (c) TiO_2/GANF.

used as substrates, following the same procedure as in the case of the pristine CNFs, for preparing TiO_2/CNF hybrid materials.

The results of the TEM analysis are shown in Fig. 4. It can be seen that in the case of GANF-ox (Fig. 4a) there is no improvement in the uniformity of the TiO_2 covering in relation to pristine GANF (Fig. 3c). Additionally, some TiO_2 aggregations can be observed, although the total TiO_2 content deposited is similar as that in the GANF sample. In the case of Gun-ei-ox, as also happens with Gun-ei, a homogeneously spread layer of TiO_2 was deposited on the CNF substrate. The different behaviour of these two oxidised nanofibres indicates that structural order (much higher for GANF-ox than for Gun-ei-ox) has more influence than the oxygen surface groups in getting a uniform TiO_2 layer.

The average diameters obtained from the analysis of TEM images for the hybrid materials with uniform TiO_2 dispersion (TiO_2/Gun-ei and TiO_2/Pyrograph) are 176 and 97 nm, with standard deviations of 44 and 11 nm, respectively. Such average diameter increases with oxidation reaching, as an example, a value of 213 ± 52 nm in the case of TiO_2/Gun-ei-ox. This increase agrees with the observation that the amount of TiO_2 in the TiO_2/Gun-ei-ox sample is a bit larger than that for TiO_2/Gun-ei (37 and 27 wt.%, respectively). Thus, the additional surface oxygen functional groups created during oxidation favour TiO_2 deposition.

The TEM values for the outer fibre diameters agree reasonably well with those obtained from SEM. As an example, in the case of TiO_2/Pyrograph, SEM analysis gives mean diameters of 117 ± 21 nm. Considering that GANF and GANF-ox do not lead to uniform TiO_2 layers, these two TiO_2/CNF materials have not been further studied.

3.4. Thermogravimetric analysis

Once observed that a homogeneous layer of TiO_2 can only be obtained on two of the three CNFs used, the reactivity in air of Pyrograph and Gun-ei has been studied. Such study is important considering that to produce TiO_2 nanofibres the CNF substrate needs to be removed and the temperature for such burning is an important parameter to be analysed. Fig. 5 shows the TGA curves in air of the Gun-ei and Pyrograph nanofibres from room temperature to 900 °C at a heating rate of 10 °C/min.

The results of the TG analysis of the CNFs indicate that the Gun-ei nanofibres start to burn in air at lower temperatures than in the case of Pyrograph nanofibres, in agreement with their much lower structural order. From these results, our first attempt was, for both samples, an air burning treatment at 450 °C for 3 h. Under such conditions, only the CNFs from the TiO_2/Gun-ei and TiO_2/Gun-ei-ox hybrids were totally burnt, whereas there was some carbon remaining in the case of TiO_2/Pyrograph (this was determined by an additional heat-treatment in a muffle up to 900 °C). Hence, for the TiO_2/Pyrograph sample, a higher temperature was used; 550 °C for 3 h, which leads to the total Pyrograph CNF removal.

3.5. TiO_2 nanofibres

Using the above indicated burning procedure, the carbon nanofibres were completely removed, leading to 100% TiO_2 samples. The morphology of the resulting TiO_2 materials, shown in Figs. 6 and 7, clearly confirms the nanotubular morphology of the obtained TiO_2 nanofibres.

These TEM images allow observing that TiO_2 nanofibres result from the growth of TiO_2 on a CNF substrate material and the subsequent burning of the CNFs in air. The mean diameters of the TiO_2 nanofibres, obtained from TEM analysis, are around 126 for Gun-ei

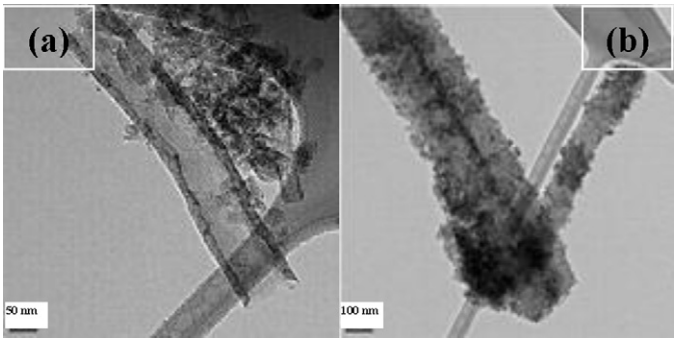

Fig. 4. TEM images of (a) TiO_2/GANF-ox and (b) TiO_2/Gun-ei-ox.

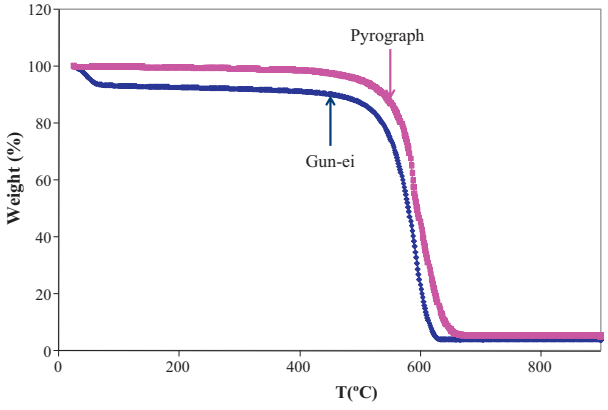

Fig. 5. TG curves of carbon nanofibres used as substrates: Gun-ei and Pyrograph.

Table 2
Textural properties of the TiO_2/CNF materials, TiO_2 contents and estimated BET surface areas.

Samples	S_{BET} (m^2/g)	DR N_2 (cm^3/g)	DR CO_2 (cm^3/g)	TiO_2 (wt.%)	S_{BET} TiO_2[a] (m^2/g)
TiO_2/Pyrograph	112	0.05	0.02	43	202
TiO_2/Gun-ei-ox	358	0.16	0.17	37	191
TiO_2/Gun-ei	375	0.17	0.18	27	181

[a] Estimated from Eq. (3).

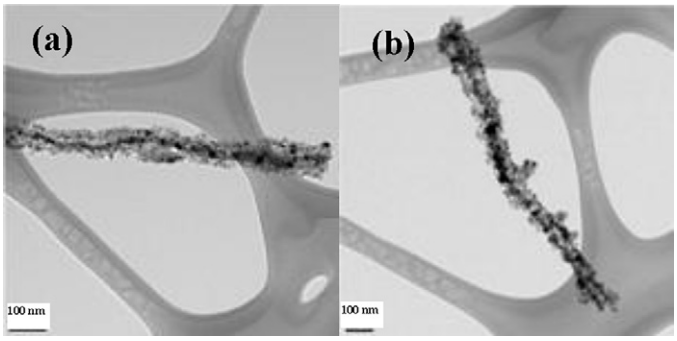

Fig. 6. TEM images of nanofibres of TiO_2 obtained from air burning of the TiO_2/CNF hybrid materials: (a) Gun-ei (3 h at 450 °C) and (b) Pyrograph (3 h at 550 °C).

CNF and 90 nm for Pyrograph CNF, with standard deviations of 27 and 14 nm, respectively.

Fig. 7a shows a detail of a SEM image of NF-TiO_2-Pyrograph with a central hollow. It can be seen that the nanofibre morphology remains after burning the Pyrograph CNF of the hybrid material. Its average diameter obtained from SEM is 101 ± 21 nm, a mean diameter which is in very good agreement with that obtained from TEM analysis.

SEM confirms the central hollows in the TiO_2 nanofibres prepared from Gun-ei-ox, with a mean diameter of 195 ± 58 nm, and that the nanotubular morphology of Gun-ei nanofibre is maintained after burning, (see Fig. 7b), with a mean diameter of 197 ± 59 nm.

3.6. Characterisation of the porous texture of TiO_2/CNF hybrids and TiO_2 nanofibres

Surface areas of the TiO_2/CNF materials and TiO_2 nanofibres are compiled, respectively, in Tables 2 and 3. BET surface areas (S_{BET}) and porous textures were determined by N_2 adsorption at −196 °C and CO_2 adsorption at 0 °C.

Table 2 shows the surface area and content of TiO_2 in TiO_2/Gun-ei, TiO_2/Gun-ei-ox and TiO_2/Pyrograph hybrid materials. Compared with original CNFs (Table 1), the surface area and the volume of micropores in TiO_2/Gun-ei and TiO_2/Gun-ei-ox are lower than those of the two CNFs used as supports. However, in the case of Pyrograph the surface area of TiO_2/Pyrograph is significantly larger than that of Pyrograph support, which indicates that the supported titania has larger surface area than the Pyrograph CNF, as it can be confirmed next.

Table 3
Textural properties of the TiO_2 nanofibres.

Samples	S_{BET} (m^2/g)	Heat treatment temperature (°C)	TiO_2 (wt.%)
NF-TiO_2-Gun-ei	29	450	100
NF-TiO_2-Gun-ei-ox	32	450	100
NF-TiO_2-Pyrograph	43	550	100

The BET specific surface area (S_{BET}) of the titania supported in all materials was estimated from the area of the hybrid material (TiO_2/CNF) and the area of original carbon nanofibres (CNF), considering the content of titania in the starting materials, according to Eq. (3):

$$S_{BET(TiO_2/CNF)} = \frac{S_{CNF}X_{CNF} + S_{TiO_2}X_{TiO_2}}{100} \quad (3)$$

where $S_{BET(TiO_2/CNF)}$, S_{CNF} and S_{TiO_2} are the specific surface areas of the hybrid materials (TiO_2/CNF), carbon nanofibres and supported TiO_2, respectively, and X_{CNF} and X_{TiO_2} are the weight percentages of the two components in each hybrid material. From this equation the estimated surface area of titania in the hybrid materials from Table 2 (S_{BET} TiO_2) was obtained.

It can be seen that only in the case of Pyrograph the estimated TiO_2 surface area (202 m^2/g) is higher than the surface area of the support (112 m^2/g). Also, it can be seen that estimated surface areas of TiO_2 in all hybrid materials, independently of the CNFs used and of their large surface area range (44–493 m^2/g), are similar, and around 190–200 m^2/g.

Following the same procedure of synthesis of the hybrid materials but without using the support, TiO_2 nanoparticles were obtained with a similar surface area (238 m^2/g) than those estimated from Eq. (3) for TiO_2 in all the hybrid materials. This implies that the presence of the carbon nanofibres does not strongly modify the surface area of the supported titanium dioxide.

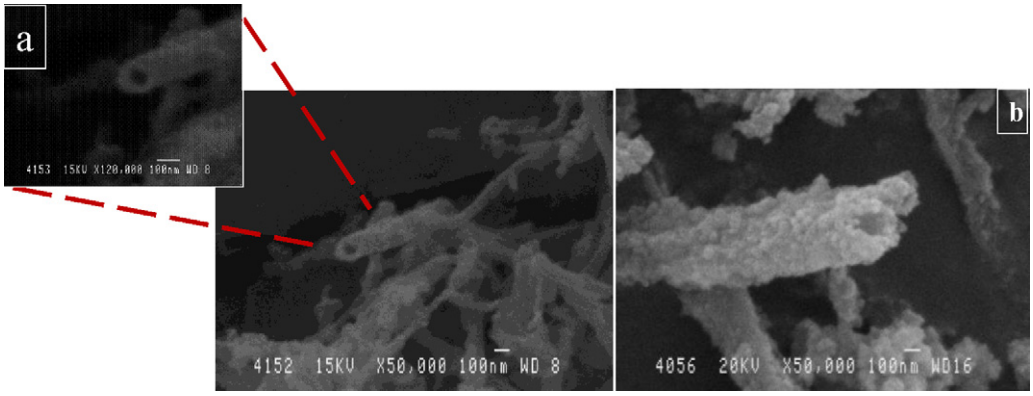

Fig. 7. SEM images showing the TiO_2 nanofibres obtained from the hybrid materials: (a) TiO_2/Pyrograph and (b) TiO_2/Gun-ei-ox, after burning Pyrograph at 550 °C and Gun-ei-ox at 450 °C for 3 h in air, respectively.

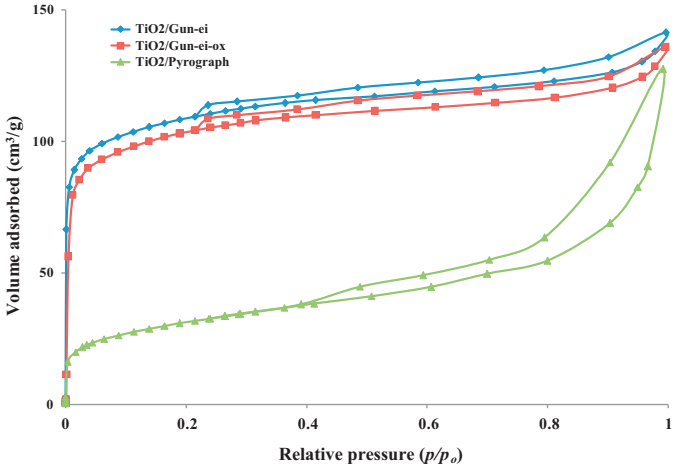

Fig. 8. Adsorption–desorption isotherms of N_2 at −196 °C on TiO_2/CNF hybrid materials prepared with uniform TiO_2 deposition.

Fig. 8 shows the nitrogen adsorption–desorption isotherms at −196 °C for the hybrid materials. TiO_2/Gun-ei and TiO_2/Gun-ei-ox show an isotherm of type I, indicating the presence of a microporous structure. In the case of TiO_2-Pyrograph, a type II isotherm with some mesopores was obtained. In comparison with original carbon nanofibres (Fig. 1) it can be observed, as commented above, that TiO_2/Gun-ei and TiO_2/Gun-ei-ox show lower nitrogen adsorbed volumes than pristine Gun-ei or Gun-ei-ox, whereas the TiO_2/Pyrograph sample has higher adsorption capacity than pristine Pyrograph sample.

Fig. 9 shows the adsorption–desorption isotherms of N_2 at −196 °C for TiO_2 nanofibres. All are type II isotherms with H3 hysteresis cycle, according to IUPAC classification [33]. The presence of H3 hysteresis is due to the presence of some mesoporosity. The specific surface areas of the synthesised TiO_2 nanofibres are in the range between 29 and 43 m^2/g (see Table 3).

Table 3 shows the porosity characterisation of the TiO_2 nanofibres prepared by air combustion of the different TiO_2/CNF composite samples.

The specific surface areas of the TiO_2 nanofibres prepared in this work are three times larger than for TiO_2 nanotubes prepared using carbon nanotubes as substrates in a previous work [16], which is important for the photocatalytic activity of these materials [33–36], and for most applications in which these materials can be applied for [37,38].

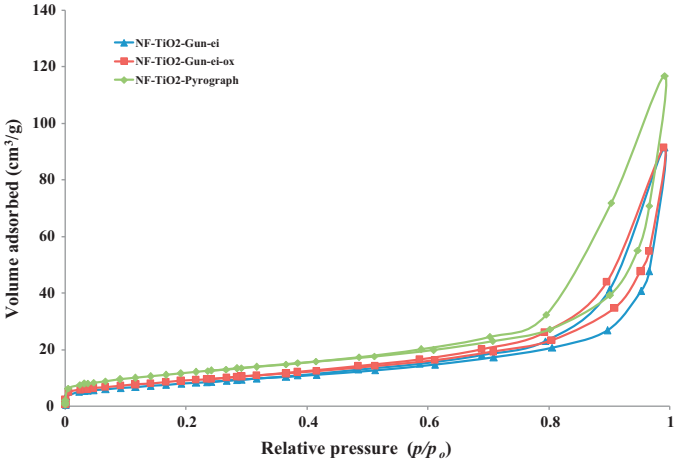

Fig. 9. Nitrogen adsorption–desorption isotherms of TiO_2 nanofibres.

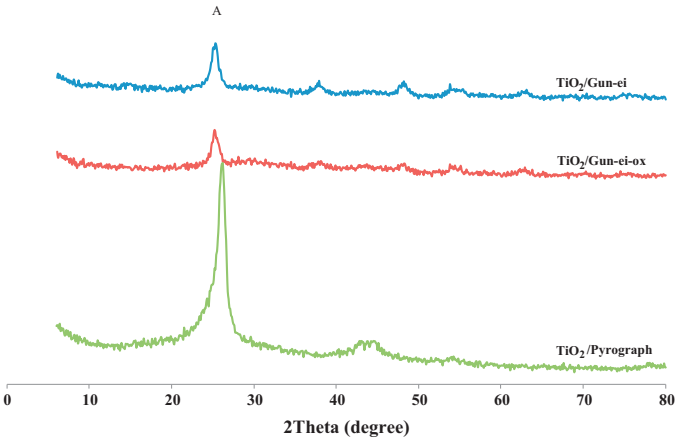

Fig. 10. XRD patterns for the TiO_2/CNF materials.

3.7. Crystalline phase characterisation

The crystalline phase composition of the TiO_2-based materials is very important from the point of view of photocatalytic activity [39]. Crystalline titanium dioxide can be present in three main phases: anatase, rutile and brookite [39], being anatase and rutile the most important ones for photocatalysis studies. Previous studies have proved that anatase is more active than rutile from a photocatalytic point of view [4,16,39].

The diffractograms of hybrid materials (TiO_2/CNF) prepared by sol–gel method and treated at 300 °C in air to induce TiO_2 crystallinity are presented in Fig. 10. The diffraction peaks of all materials (TiO_2/Gun-ei, TiO_2/Gun-ei-ox and TiO_2/Pyrograph) are mostly related to the presence of anatase phase in all hybrid materials. However, the main anatase peak in the XRD patterns of the TiO_2/Pyrograph hybrid material overlaps with the largest reflection peak of Pyrograph nanofibres, and it is hard to deduce the crystalline size of anatase for TiO_2/Pyrograph. The average size of the crystallites for the hybrid materials TiO_2/Gun-ei and TiO_2/Gun-ei-ox was estimated from the main anatase XRD peak to be ~9 nm.

The presence of anatase phase indicates that these materials would be, in principle, photocatalytically active [4].

Fig. 11 shows the XRD patterns of the resulting TiO_2 nanofibres (heat-treated in air at 450 °C and 550 °C to remove the carbon nanofibres). These patterns show the absence of the d_{002} diffraction peak in the corresponding XRD pattern of Pyrograph nanofibres. Similarly to the hybrid materials (TiO_2/CNFs), all sharp peaks observed in the XRD patterns of TiO_2 nanofibres belong to anatase

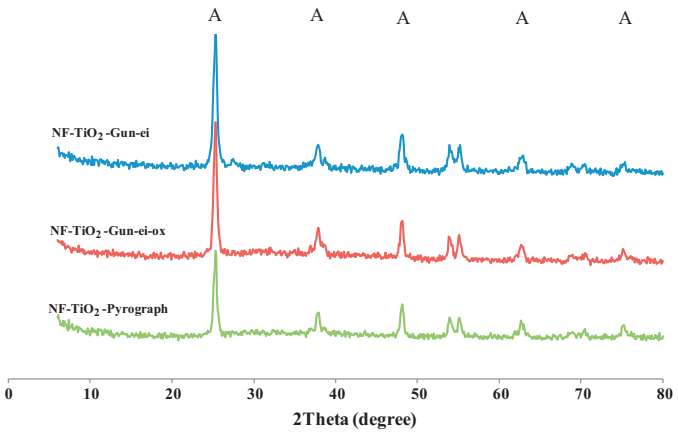

Fig. 11. XRD patterns for the TiO_2 nanofibres.

Table 4
Conversion of propene (100 ppmv) by TiO_2/CNFs and TiO_2-nanofibres, using two stream flow rates: 30 and 60 ml/min.

Samples	Conversion at 30 ml/min (%)	Conversion at 60 ml/min (%)
TiO_2/Gun-ei	28	14
NF-TiO_2-Gun-ei	24	9
TiO_2/Gun-ei-ox	43	36
NF-TiO_2-Gun-ei-ox	30	15
TiO_2/Pyrograph	34	25
NF-TiO_2-Pyrograph	23	9

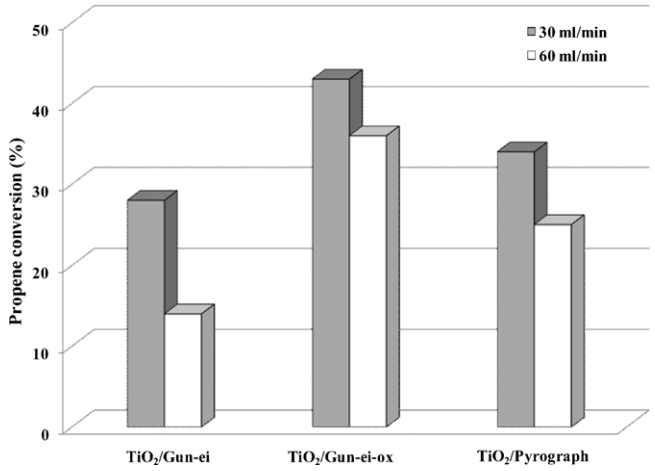

Fig. 12. Oxidation of propene by hybrid materials using two flow rates (30 and 60 ml/min).

phase (diffraction peaks of anatase (JCPDS no. 21–1272) appear at 25.3°, 37.8°, 48.0°, 53.9°, 55.1°, 62.7° and 70.4°).

As expected, the thermal treatment over the hybrid materials (performed at 450 °C or 550 °C), performed for obtaining TiO_2 nanofibres results in an increase in the crystallinity and average crystal size. The mean anatase crystalline sizes was estimated applying the Scherrer formula to the main XRD peak ($2\theta = 25.3$), resulting about 17–19 nm for all the samples.

3.8. Photocatalytic activity for propene oxidation at low concentration

Photocatalytic experiments were performed by passing the propene stream through the photocatalyst bed until propene concentration in the outlet stream equalled the inlet concentration. Then, the UV-light was switched on and the decrease in the propene concentration over time was recorded. The results of photocatalytic activity of propene at 100 ppmv of all samples are shown in Table 4 for the two flow rates, 30 and 60 ml/min.

From Table 4 it can be seen that: (i) all TiO_2 samples prepared in this work are considerably active due to the presence of anatase phase in all of them, (ii) their photocatalytic activity increases in the order: NF-TiO_2-Pyrograph ≤ NF-TiO_2-Gun-ei TiO_2-Gun < NF-TiO_2-Gun-ei-ox < TiO_2/Pyrograph < TiO_2/Gun-ei-ox, (iii) all the hybrid materials are more active than their corresponding TiO_2 nanofibres, (iv) the CNFs oxidation enhances the photocatalytic activity of the hybrid materials, being the sample TiO_2/Gun-ei-ox the most active one, as shown in Fig. 12, and (v) the photocatalytic activity decreases, as expected, when the flow rate increases.

The amount of CO_2 generated in the oxidation of propene has been quantified and compared with the oxidised propene. Thus, the ratio mol of CO_2 generated/mol of propene oxidised is around 3 in all the experiments, which indicates total mineralisation of the oxidised propene to carbon dioxide and water, according to previously published results dealing with propene oxidation [16,28,29,32].

The data of Table 4 reveal, independently of the flow rate used, the important and beneficial role played by the CNFs of the hybrid materials in their resulting photocatalytic activity. In addition of their suitable thermal and electrical conducting properties, that help the transfer of electrons from TiO_2 to CNF enhancing the photocatalytic oxidative reactivity, the CNFs surface area is also useful. Two are the main advantages of the presence of CNFs: (i) they act as adsorbents that concentrate the molecules to be oxidised and (ii) they act as dispersing agents, stabilising the TiO_2 particles and preventing their agglomeration. As a result, the presence of CNFs in hybrid materials, compared with the NF-TiO_2 materials, provides higher photocatalytic activity.

A comparative study of the effect of the different CNFs used can be seen in Fig. 12, that displays the photocatalytic activity of the three hybrid materials; TiO_2/Gun-ei, TiO_2/Gun-ei-ox, TiO_2/Pyrograph. It can be observed that the photocatalytic activity for the oxidation of propene at low concentration (100 ppmv) of TiO_2/Gun-ei is the lowest, whereas that for TiO_2/Gun-ei-ox is the largest one, being this sample even more active than TiO_2 carbon hybrids prepared in a previous work [16] using carbon nanotubes.

The larger photocatalytic activity of TiO_2/Pyrograph in relation to TiO_2/Gun-ei cannot be attributed to the hybrid's surface area, which is three times lower for TiO_2/Pyrograph than for TiO_2/Gun-ei (Fig. 8 and Table 2). Its higher activity could be due to several reasons: (i) to the slightly larger TiO_2 surface area in TiO_2/Pyrograph and/or to a smaller anatase crystalline phase in TiO_2/Pyrograph, (ii) to the presence of a larger volume of mesopores in the Pyrograph CNF, that would enhance the migration of the molecules of propene adsorbed on the TiO_2 surface, favouring propene oxidation and/or (iii) to its higher degree of crystallinity (Fig. 2) and hence of conductivity.

It is well known that the photocatalytic reaction occurs on the surface of the catalysts, and recombination of the photogenerated electrons and holes is very fast, so interfacial charge carrier transfer is possible only when the donor or acceptor is pre-adsorbed before the photocatalytic reaction.

The higher photocatalytic activity of TiO_2/Gun-ei-ox compared to TiO_2/Gun-ei cannot be attributed to their surface areas, since both are quite similar. It may be attributed to large quantities of highly reactive radicals, including the hydroxyl radical •OH, that lead to a more uniformly covered and active TiO_2 photocatalyst.

Considering the fact that TiO_2/Pyrograph presents higher activity than TiO_2/Gun-ei, it would have been very interesting to oxidise Pyrograph and prepare the corresponding hybrid material. Unfortunately, we ran out of sample and we could not perform such tests. Nevertheless, we could do it with another Pyrograph sample, with smaller BET surface area, that will be refer to as Pyrograph-b, from which we could obtain the following conclusions:

- A uniform TiO_2 layer can be obtained on Pyrograph-b using the procedure already explained.
- Oxidation of Pyrograph-b leads to a material that can be used for preparing a TiO_2/Pyrograph-b-ox hybrid material with uniform TiO_2 deposition and slightly larger TiO_2 content than when Pyrograph-b is used as support.
- Photocatalytic activity of TiO_2/Pyrograph-b-ox is larger than that of TiO_2/Pyrograph-b.

These results confirm Pyrograph as a very good support for our photocatalytic application, possibly due to its moderate crystallinity and textural characteristics.

In relation to the photocatalytic results of the TiO_2 nanofibres obtained by thermal treatment in air of the hybrid materials, it was shown (in Table 4) that they are lower than those of their

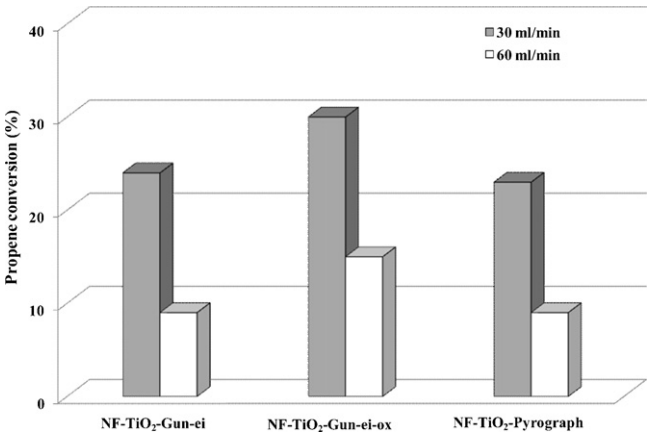

Fig. 13. Oxidation of propene using two flow rates (30 and 60 ml/min) for the TiO_2 nanofibres.

corresponding hybrid materials. Fig. 13 compares the photocatalytic activities of these NF-TiO_2 materials. From the figure it can be seen again that NF-TiO_2-Gun-ei-ox, in comparison to the other TiO_2 nanofibres prepared, presents the highest activity. This might be probably due to the surface functional groups generated by oxidation, which could be preserved after burning the CNFs in the hybrid material (TiO_2/Gun-ei-ox).

Interestingly, in comparison with a previous work [16] dealing with CNTs, the use of CNFs gives better photocatalytic activities. Since both CNTs and CNFs present similar TiO_2 anatase phases, it can be deduced that the greater surface area of the CNFs is a key variable. Further activity enhancements will require to work on the use of higher surface area CNFs and on modifying the anatase–rutile ratio, according to previous results that show that anatase with a small percentage of rutile is more active than pure anatase, as it is the case in Degussa P25 [40–42].

4. Conclusions

This study shows that anatase TiO_2/CNF hybrid materials and anatase TiO_2 nanofibres can be obtained successfully by sol–gel synthesis using carbon nanofibres as substrate materials and titanium alkoxide as TiO_2 precursor, being the characteristics of the CNFs important for the characteristics of the TiO_2 covering on the CNFs. Thus, a dense and homogenous layer of TiO_2 can be obtained only when CNFs with low or moderate crystallinity (Gun-ei and Pyrograph) are used as substrates, but not when a high crystallinity CNF (GANF) is used. An oxidation of the CNFs prior to TiO_2 deposition leads to an increase in the total TiO_2 amount deposited, in comparison to pristine CNFs. Additionally, for the pristine CNFs where a uniform TiO_2 layer is obtained (Pyrograph and Gun-ei), an oxidation treatment also leads to a uniform TiO_2 deposition. However, oxidation of GANF does not lead to a support that is able to get a uniform TiO_2 layer, in the conditions used in the present study.

An explanation that can help to understand why only amorphous carbon nanofibres lead to a homogeneous TiO_2 covering can be based on the fact that the amorphous carbon nanofibres have more defects than the more crystalline ones. Defects of the amorphous carbon nanofibres would be the nucleation points for the TiO_2 deposition, and considering the larger amount of defects all along the surface of the amorphous carbon nanofibres, a more homogeneous layer of TiO_2 would be obtained on such supports. On the contrary, the crystalline CNFs have less defects, and TiO_2 is deposited only on them in a first step and, subsequently, on the deposited titanium dioxide, leading to coverings as those obtained in the present work on crystalline CNFs.

The removal of the carbon nanofibres in hybrid materials (TiO_2/CNFs) with uniform TiO_2 layer by combustion leads to TiO_2 nanofibres with small crystal size of anatase and high surface area, compared to TiO_2 nanotubes obtained in a previous study.

The prepared materials have shown a significant photocatalytic activity, being the composite materials the most interesting materials amongst those prepared, due to the role of carbon nanofibres in the stability of the small crystalline size of anatase and in the adsorption of the pollutants to be oxidised. The photocatalytic activity can be further improved by increasing the surface area of the prepared materials and trying to have a mixture of anatase and rutile with a similar ratio than in TiO_2-P25.

Acknowledgments

M. Ouzzine thanks MAEC-AECID for a predoctoral fellowship. The authors thank Generalitat Valenciana (GVPRE/2008/004, Prometeo/2009/047 and FEDER), and Office of the Vice President for Research, Development and Innovation of University of Alicante (UAUSTI10-08) for financial support.

References

[1] H.G. Yang, C.C. Sun, S.Z. Qiao, J. Zou, G. Liu, S.C. Smith, et al., Nature 453 (7195) (2008) 638–641.
[2] A. Fujishima, K. Honda, Nature 238 (5358) (1972) 37–38.
[3] R. Buonsanti, V. Grillo, E. Carlino, C. Giannini, T. Kipp, R. Cingolani, et al., Journal of the American Chemical Society 130 (33) (2008) 11223–11233.
[4] M. Inagaki, T. Imai, T. Yoshikawa, B. Tryba, Applied Catalysis B: Environmental 51 (4) (2004) 247–254.
[5] G. Cappelletti, S. Ardizzone, C.L. Bianchi, S. Gialanella, A. Naldoni, C. Pirola, et al., Nanoscale Research Letters 4 (2) (2009) 97–105.
[6] B. Ahmmad, Y. Kusumoto, S. Somekawa, M. Ikeda, Catalysis Communications 9 (6) (2008) 1410–1413.
[7] X.-H. Xia, Z.-Y. Jia, Y. Yu, Y. Liang, Z. Wang, L.-L. Ma, Carbon 45 (4) (2007) 717–721.
[8] T.Y. Lee, P.S. Alegaonkar, J.-B. Yoo, Thin Solid Films 515 (12) (2007) 5131–5135.
[9] M. Sánchez, R. Guirado, M.E. Rincón, Journal of Materials Science – Materials in Electronics 18 (11) (2007) 1131–1136.
[10] L.-R. Hou, C.-Z. Yuan, Y. Peng, Journal of Hazardous Materials 139 (2) (2007) 310–315.
[11] P. Fu, Y. Luan, X. Dai, Journal of Molecular Catalysis A: Chemical 221 (1–2) (2004) 81–88.
[12] S. Gelover, P. Mondragón, A. Jiménez, Journal of Photochemistry and Photobiology A: Chemistry 165 (1–3) (2004) 241–246.
[13] B. Tryba, A.W. Morawski, M. Inagaki, Applied Catalysis B: Environmental 41 (4) (2003) 427–433.
[14] Y. Xie, S.H. Heo, S.H. Yoo, G. Ali, S.O. Cho, Nanoscale Research Letters 5 (3) (2010) 603–607.
[15] B. Gao, G.Z. Chen, G.L. Puma, Applied Catalysis B: Environmental 89 (3–4) (2009) 503–509.
[16] N. Bouazza, M. Ouzzine, M.A. Lillo-Ródenas, D. Eder, A. Linares-Solano, Applied Catalysis B: Environmental 92 (3–4) (2009) 377–383.
[17] G. Hu, X. Meng, X. Feng, Y. Ding, S. Zhang, M. Yang, Journal of Materials Science 42 (17) (2007) 7162–7170.
[18] S. Kim, S.K. Lim, Applied Catalysis B: Environmental 84 (1–2) (2008) 16–20.
[19] J.-Y. Gong, S.-R. Guo, H.-S. Qian, W.-H. Xu, S.-H. Yu, Journal of Materials Chemistry 19 (7) (2009) 1037–1042.
[20] S. Anandan, M. Yoon, Journal of Photochemistry and Photobiology C: Photochemistry Reviews 4 (2003) 5–18.
[21] L. Hu, J. Lv, S. Chen, Z. Guo, Nanoscience 11 (3) (2006) 175–178.
[22] T.W. Ebbesen, H.J. Lezec, H. Hiura, J.W. Bennett, H.F. Ghaemi, T. Thio, Nature 382 (6586) (1996) 54–56.
[23] C.-Y. Kuo, Journal of Hazardous Materials 163 (1) (2009) 239–244.
[24] S. Wang, L. Ji, B. Wu, Q.M. Gong, Y.F. Zhu, J. Liang, Applied Surface Science 255 (2008) 3263–3266.
[25] J. Rouquerol, F. Rouquerol, K.S.W. Sing, Adsorption by Powders and Porous Solids: Principles, Methodology and Applications, Academic Press, San Diego, 1999.
[26] D. Cazorla-Amorós, J. Alcañiz-Monge, A. Linares-Solano, Langmuir 12 (11) (1996) 2820–2824.
[27] A. Linares-Solano, J. Alcañiz-Monje, C. Salinas-Martínez de Lecea, D. Cazola-Amorós, Tanso 185 (1998) 316–325.
[28] N. Bouazza, M.A. Lillo-Ródenas, A. Linares-Solano, Applied Catalysis B: Environmental 77 (3–4) (2008) 284–293.
[29] N. Bouazza, M.A. Lillo-Ródenas, A. Linares-Solano, Applied Catalysis B: Environmental 84 (3–4) (2008) 671–698.
[30] C.T. Brigden, S. Poulston, M.V. Twigg, A.P. Walker, A.J.J. Wilkins, Applied Catalysis B: Environmental 32 (1–2) (2001) 63–71.

[31] F.W. Lurmann, H.H. Main, Analysis of the ambient VOC data collected in the Southern California Air Quality Study, Report Prepared for the California Air Resources Board, Sacramento, CA by Sonoma Technology Inc., Santa Rosa, CA, STI-99120-1161-FR, Contract no. A823-130, February 1992.
[32] M.A. Lillo-Ródenas, N. Bouazza, A. Berenguer-Murcia, J.J. Linares-Salinas, P. Soto, A. Linares-Solano, Applied Catalysis B: Environmental 71 (3–4) (2007) 298–309.
[33] K.S.W. Sing, D.H. Everett, R.A.W. Haul, L. Moscou, R.A. Pierotti, J. Rouquerol, et al., Pure and Applied Chemistry 57 (1985) 603–619.
[34] F. Suarez-Garcia, E. Vilaplana-Ortego, M. Kunowsky, M. Kimura, A. Oya, A. Linares-Solano, International Journal of Hydrogen Energy 34 (22) (2009) 9141–9150.
[35] J.C. Xu, M. Lu, X.Y. Guo, H.L. Li, Journal of Molecular Catalysis A: Chemical 226 (1) (2005) 123–127.
[36] S.G. Yang, X. Quan, X.Y. Li, Journal of Environmental Sciences 17 (2) (2005) 290–293.
[37] A.Y. Kawde, A. Vats, R.V. Shende, J.A. Puszynski, Technical Proceedings of the 2011 NSTI Nanotechnology Conference and Expo, NSTI-Nanotech, 2011, pp. 747–750.
[38] M.P. Neupane, I.S. Park, T.S. Bae, H.K. Yi, M. Uo, F. Watari, M.H. Lee, Journal of Materials Chemistry 21 (32) (2011) 12078–12082.
[39] C.-H. Lu, W.-H. Wu, R.B. Kale, Journal of Hazardous Materials 154 (1–3) (2008) 649–654.
[40] D.C. Hurum, A.G. Agrios, K.A. Gray, T.M.C. Rajh, Thurnauer 107 (19) (2003) 4545–4549.
[41] P. Deak, B. Aradi, T. Frauenheim, Journal of Physical Chemistry C 115 (8) (2011) 3443–3446.
[42] T.A. Kandiel, A. Feldhoff, L. Robben, R. Dillert, D.W. Bahnemann, Chemistry of Materials 22 (1) (2010) 2050–2060.